Third Normal Stress Difference and Component Relaxation Spectra for Bidisperse Melts under Oscillatory Shear

Julia A. Kornfield† and Gerald G. Fuller*

Chemical Engineering Department, Stanford University, Stanford, California 94305

Dale S. Pearson

Department of Chemical and Nuclear Engineering and Materials Department, University of California, Santa Barbara, California 93106

Received January 24, 1991; Revised Manuscript Received May 8, 1991

ABSTRACT: A recently developed rheooptical technique that simultaneously measures infrared dichroism and birefringence is used to study bidisperse, linear polymer melts in an oscillatory shear. The method was used to individually measure the contribution of the high and low molecular weight components to the third normal stress difference. This was accomplished by measuring the infrared dichroism due to deuterium-labeled polymers. Binary blends are prepared from nearly monodisperse pairs of hydrogenated and deuteriated polyisoprenes of molecular weights 53 000 and 370 000 with volume fractions of long polymer, Φ_L, of 0.10, 0.20, 0.30, 0.50, and 0.75. The long-chain relaxation in the blends shows the appearance of a peak for compositions with $\Phi_L \leq 0.50$ at approximately the same frequency as a similar peak in the pure short polymer. The response of the short-chain relaxation in the blends shows the appearance of a low-frequency shoulder that becomes surprisingly large as the volume fraction of long chains increases. The results are used to test a modified reptation model that includes constraint release and a short-range orientational coupling between chain segments.

1. Introduction

Polydispersity strongly affects the viscoelastic properties of entangled linear polymer melts and solutions. To avoid the complexity of these effects in an arbitrary molecular weight distribution, bidisperse systems composed of two sharply defined molecular weights, long (L) and short (S) chains, are often used as model systems for investigation. Many of these studies have been made with the objective of determining empirical "blending laws" for the rheological properties.[1-3] More recent experiments have been performed to clarify the effect of polydispersity on the relaxation of each species in binary blends of polymers with widely separated molecular weights ($M_L \gg M_S$), each well above the entanglement molecular weight ($M_S > 20M_e$).[4] Monodisperse entangled polymers have a narrow distribution of relaxation times, which is fairly well understood in terms of the reptation theory.[5] As a consequence, a well-defined peak appears in the loss modulus, $G''(\omega)$, of these polymers ($M \gg M_e$) with magnitude G_m'' at frequency ω_m. The peak frequency varies as the reciprocal of the terminal relaxation time τ, with $\tau\omega_m \approx 2$ observed for monodisperse polymers. The terminal relaxation time τ, with $\tau\omega \approx 2$ observed for monodisperse polymers. The terminal relaxation time is also found to be proportional to $M^{3.4}$, although the original reptation theory predicts a M^3 dependence. For binary blends with sufficiently large volume fractions of long polymer, $\Phi_L > 0.5$, there are two peaks in $G''(\omega)$ when both components are entangled and M_L/M_S is significantly greater than unity.[4] The peak frequencies are close to those found for the pure long and short components, ω_L and ω_S. The magnitude of the low-frequency peak, G_L'', increases and that of the high-frequency peak, G_S'', decreases as Φ_L increases.

The observation that the characteristic relaxation times of the individual components determine the two time scales of relaxation in the bidisperse melt is consistent with the reptation theory. Curvilinear diffusion of a chain over a distance equal to its own mean contour length determines the longest relaxation time of a particular molecular weight chain in the reptation model. Provided that the diffusion of the chain is not affected by polydispersity, this leads to a spectrum of relaxation times for a binary blend that has two characteristic relaxation times equal to those of the monodisperse components. Reptation theory does not, however, describe the nonlinear dependence of the magnitudes G_S'' and G_L'' on Φ_L. As long chains are added to a short-chain melt, the loss peak at high frequency (the S peak) is only slightly affected until a substantial volume fraction of long polymer is reached, then G_S'' decreases rapidly as Φ_L increases until it disappears for $\Phi_L = 1$. The magnitude of relaxation at low frequency (the L peak) also shows a nonlinear dependence on Φ_L: the L peak is not evident until approximately 50% volume of long polymer is present, and then G_L'' increases strongly, roughly as Φ_L^2.

The nonlinear dependence of the magnitude of the S and L peaks indicates that the contribution of the short and long polymers is not simply additive as in the original reptation theory. A more consistent molecular model can be obtained by allowing both species to relax not only by reptation but also by the release of entanglements due to the motion of surrounding chains. This allows part of the stress contributed by the long polymer to relax on the time scale of short-chain reptation, τ_S, considerably faster than its own reptation time. Reptation-based theories that incorporate constraint release have been developed,[6-13] including a recent model by Rubinstein, Helfand, and Pearson (RHP), that successfully describes the increase in G_L'' as Φ_L^2. These theories predict not only the rheological properties but also the contribution of each molecular weight component to the bulk viscoelasticity.

A more stringent test of these molecular models can be made by determining the relaxation of each component as well as the bulk. This can be accomplished by using optical techniques in conjunction with mechanical testing.

* To whom correspondence should be addressed.
† Present address: Chemical Engineering, California Institute of Technology, Pasadena, California 91125.

0024-9297/91/2224-5429$02.50/0

For this purpose, simultaneous infrared dichroism and birefringence measurements were used in an initial study of the relaxation of a blend and both of its components following a step strain.[14] We now report complementary measurements of relaxation using oscillatory shear. In a separate paper, the frequency dependence of the third normal stress difference measured by using oscillatory flow birefringence was presented and compared to mechanical measurements of the dynamic moduli, G' and G''.[15]

In this paper we report the degree of orientation of each component as a function of frequency using infrared dichroism measurements. Some additional conclusions based on the birefringence measurements are also reported. After the materials and methods are described, the optically measured normal stress relaxation spectra are presented in section 3, and the results for the relaxation spectra of the long and short chains are presented in section 4. Then the observed component relaxations are compared to the predictions of the Rubinstein–Helfand–Pearson model of reptation and constraint release. The final section summarizes the implications of these results for the effects of polydispersity on melt rheology.

2. Materials and Methods

The polymer system and experimental apparatus used for infrared dichroism and birefringence measurements were previously described in our study of the step strain relaxation of binary blends.[14] The theoretical background of the optical measurements, the construction of the optical train, and the synthesis and characterization of the polymers are presented in that paper. For this work, a new flow cell that performs sinusoidal shear is employed, which is also described elsewhere.[15]

Saturated derivatives of ionically polymerized polyisoprenes with two degrees of polymerization were synthesized by L. J. Fetters: "short" chains of 780 and "long" chains of 5440 isoprene monomer units, both many times the entanglement molecular weight ($M_S/M_e \approx 29$ and $M_L/M_e \approx 205$, where M_S and M_L denote the molecular weight of the short and long chains and M_e is the molecular weight between entanglements). For each degree of polymerization, two derivatives are used: normal (hydrogenated polyisoprene, HPI) and labeled (deuteriated polyisoprene, DPI). The normal and labeled polymers of a given length differ only in the substitution of a fraction of the hydrogen with deuterium; they have identical rheological properties and negligible potential for phase separation.[14]

The infrared spectra of the two derivatives are shown in a previous paper.[14] Optical measurements are performed by using an infrared diode laser with a wavelength corresponding to that of the carbon–deuterium (C–D) bond stretching absorption peak. This provides a means to measure the orientation of labeled chains in a binary blend. Specifically, the anisotropic attenuation of light by the sample (dichroism) arises solely from the anisotropic orientation of C–D bonds along the labeled chain.

The bidisperse samples used in this work are the same as those employed in the earlier experiments on step strain relaxation. Blends of the two components were prepared with various volume fractions of long polymer: $\Phi_L = 0.1, 0.2, 0.3, 0.5$, and 0.75. Three samples were prepared for each value of Φ_L: an unlabeled blend for the dynamic modulus measurements and long-chain labeled and short-chain labeled blends for the birefringence and dichroism measurements. The methods used for the oscillatory shear optical testing have been described previously, along with mechanical measurements of the dynamic moduli of these blends.[15]

All the optical experiments were conducted at room temperature. Above 25 rad/s the servo controller was unstable, and this imposed the upper limit on frequency for the optical measurements reported here. For frequencies between 1 and 25 rad/s, a strain amplitude of 15% was found to be the lowest magnitude possible to achieve sufficient birefringence and dichroism signals for the blends. At lower frequencies the amplitude was increased to 30%. Measurements on the pure components were made using labeled (short only) and unlabeled samples. With label present, agreement was found between the dichroism and birefringence of the monodisperse short polymer. This indicates that the orientational anisotropies measured by the two quantities are the same in a monodisperse system, where the dynamics of the labeled chains (measured by dichroism) are identical with those of the bulk (measured by birefringence). Unlabeled pure polymer was also used for birefringence measurements because a larger gap can be used, giving better signal to noise than with labeled samples, even with much smaller strains (less than 5% at all frequencies).

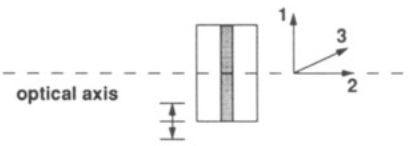

Figure 1. Flow cell geometry showing the optical axis parallel to the 2-axis and normal to the parallel plates of the shear flow cell, shown as open rectangles. Shear is applied to the sample between the plates by translating one of the rock salt plates in the 1-direction as indicated.

3. Birefringence Measurement of Normal Stress

For sinusoidal shearing with frequency ω, the velocity gradient $\dot{\gamma} \equiv dv_1/dx_2$ can be written:

$$\dot{\gamma} = \mathrm{Re}\,(\dot{\gamma}^0 e^{i\omega t}) \tag{3.1}$$

The nonzero components of the stress tensor are then

$$\tau_{12} = \tau_{21} = \mathrm{Re}\,(\tau_{12}{}^0 e^{i\omega t}) \tag{3.2}$$

$$\tau_{ii} = \mathrm{Re}\,(\tau_{ii}{}^0 e^{i2\omega t}) + d_i \tag{3.3}$$

where $i = 1, 2, 3$, the superscript zero quantities are complex amplitudes, and the d_i quantities are scalar displacements. In the small-amplitude limit, the usual viscoelastic functions η^* and Ψ_1^* are used to describe the stress–strain relationships as functions of ω.[16] The following equations define the dynamic viscosity $\eta^* = \eta' - i\eta''$

$$\tau_{12}{}^0 = \eta^* \dot{\gamma}^0 \tag{3.4}$$

the complex amplitude for the first normal stress difference, $\Psi_1^* = \Psi_1' - i\Psi_1''$

$$\tau_{11}{}^0 - \tau_{22}{}^0 = \Psi_1^* (\dot{\gamma}^0)^2 \tag{3.5}$$

and the displacement coefficient for the first normal stress, $\Psi_1{}^d$

$$d_1 - d_2 = \Psi_1{}^d |\dot{\gamma}^0|^2 \tag{3.6}$$

The complex amplitude and displacement of the third normal stress difference, Ψ_3^* and $\Psi_3{}^d$, are analogously defined to describe $\tau_{11} - \tau_{33}$.

In response to stress, the optical properties of a polymeric liquid become anisotropic due to the orientation of the polymer molecules. In this work the anisotropic retardation of light (birefringence) and the anisotropic attenuation of light (dichroism) are measured simultaneously. The latter is amenable to infrared labeling and has been used to study the dynamics of each molecular weight component in these blends; those results are presented in section 4. In this section the birefringence results, related to the bulk state of stress in the polymer, are briefly discussed so that they may be compared with model predictions in section 5.3.2.

In our choice of flow cell geometry, the optical measurements are preformed with light propagating across the gap of the flow cell, as shown in Figure 1. In this orientation, the beam samples the 1,3-projection of the refractive index tensor.[17] Therefore, the birefringence in our experimental geometry is related by the stress optical

rule to $\tau_{11} - \tau_{33}$:

$$\Delta n' = C(\tau_{11} - \tau_{33}) = \mathrm{Re}\,(C[\tau_{11}^{0} - \tau_{33}^{0}]e^{i2\omega t}) + C[d_1 - d_3] \tag{3.7}$$

where C is the stress–optical coefficient. Like the normal stresses, the 1,3-birefringence may be written in terms of a complex amplitude, $\Delta n'^* = (\Delta n')' - i(\Delta n')''$, and a scalar displacement, $(\Delta n')^d$, defined as follows:

$$\Delta n'^* = \frac{C[\tau_{11}^{0} - \tau_{33}^{0}]}{(\dot\gamma^0)^2} = C\Psi_3^* \tag{3.8}$$

$$(\Delta n')^d = \frac{C[d_1 - d_3]}{|\dot\gamma^0|^2} = C\Psi_3^{\,d} \tag{3.9}$$

In these experiments a sinusoidal shear strain $\gamma(t) = \gamma_0 \sin \omega t$ is applied; from the definition of $\dot\gamma^0$ this gives $\dot\gamma^0 = \gamma_0\omega$, hence

$$\Delta n'(t) = \gamma_0^2\omega^2(\Delta n')' \cos 2\omega t + \gamma_0^2\omega^2(\Delta n')'' \sin 2\omega t + \gamma_0^2\omega^2(\Delta n')^d \tag{3.10}$$

From the measured birefringence, the magnitudes of the oscillatory components and the displacement, $\omega^2(\Delta n')'$, $\omega^2(\Delta n')''$, and $\omega^2(\Delta n')^d$, are determined. The results of these small-strain amplitude measurements have been presented previously and support the following constitutive relationships between the normal stress differences and the shear stress:[15]

$$-\omega^2\Psi_1'(\omega) = G'(\omega) - (1/2)G'(2\omega) \tag{3.11}$$

$$\omega^2\Psi_1''(\omega) = G''(\omega) - (1/2)G''(2\omega) \tag{3.12}$$

$$\omega^2\Psi_1^{\,d} = G' \tag{3.13}$$

$$(\tau_{22} - \tau_{33}) = -\beta(\tau_{11} - \tau_{22}) \tag{3.14}$$

where $G^*(\omega)$ is the dynamic modulus, related to η^* by $G^* = i\omega\eta^*$. These relationships are predicted by many constitutive equations (allowing models with $\beta = 0$), including all models that show simple fluid behavior in the limit of linear viscoelasticity.[18] Since $(\Delta n')^* = C\Psi_3^* = c'\Psi_1^*$ (from the stress–optical rule and eq 3.14), the magnitude of the real part of the complex amplitude of the birefringence multiplied by the squared frequency, $\omega^2(\Delta n')'$, is related to the storage modulus (see eq 3.11), and the imaginary part, $\omega^2(\Delta n')''$, is related to the loss modulus (see eq 3.12). The displacement component, $\omega^2(\Delta n')^d$, is simply proportional to the storage modulus (eq 3.13). The birefringence results have been presented in detail previously[15] but are repeated here for comparison with the component dynamics and with model predictions. The results are shown in part a of Figures 2–4: Figure 2a, $-\omega^2(\Delta n')'$; Figure 3a, $\omega^2(\Delta n')''$; Figure 4a, $\omega^2(\Delta n')^d$. Part b of Figures 2–4 show the predictions of the model described in section 5. The logarithm of the absolute value of $-\omega^2(\Delta n')'$ is shown in Figure 4 because this quantity changes sign for some melts as a function of frequency. Two curves are shown for those samples with positive and negative portions as indicated in the legend.

4. Infrared Dichroism Measurement of Long- and Short-Chain Relaxation

The motivation for employing an optical technique to study the effect of polydispersity is to access the dynamics of an individual molecular weight component by use of an optical labeling technique. In this case, lightly deuteriated derivatives of each species are used as the labeled component. Attenuation of light due to the C–D bond stretching absorption arises only from the labeled chains;

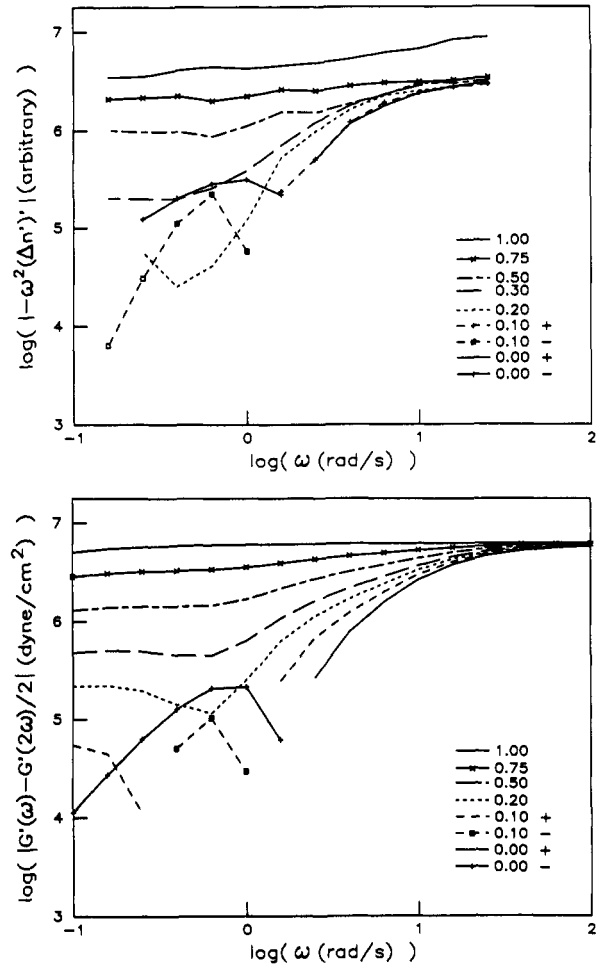

Figure 2. (a, Top) Measured frequency dependence of the real part of the complex amplitude of the third normal stress difference using 1,3-birefringence. Curves shown connect the data points. For the blends in which $-\omega^2(\Delta n')'$ changes sign, positive and negative portions are distinguished as indicated in the legend. (Reproduced from ref 15.) (b, Bottom) RHP model prediction for the real part of the complex amplitude of the first normal stress difference on a scale appropriate for comparison with the optical measurements in (a).

dichroism at this wavelength provides a measure of the anisotropic orientation of C–D bonds due to the local orientation of the labeled chains. The 1,3-dichroism in our experiments has the same form as the birefringence signal (see eq 3.10), with oscillatory parts having twice the frequency of the imposed shear plus a steady component:

$$\Delta n''_K(t) = \gamma_0^2\omega^2(\Delta n''_K)' \cos 2\omega t + \gamma_0^2\omega^2(\Delta n''_K)'' \sin 2\omega t + \gamma_0^2\omega^2(\Delta n''_K)^d \tag{4.1}$$

where $\Delta n''_K$ is the dichroism with K chains (either L or S) labeled. From here on we use the notation $K \equiv \Delta n''_K$ ($K = L$ or S).

According to the theory of rubber elasticity, the anisotropic orientation distribution and the stress are related in the same way to the free energy. In this view, the dichroism arising from the orientation of a labeled component in a melt is proportional to the contribution of that species to the stress tensor.

A considerable body of evidence indicates that a probe molecule with an anisotropic shape in a polymer matrix remains oriented as long as the matrix is oriented.[19–24] When such local orientational coupling is included in the theory of orientation and stress in strained rubber, it is found that in the long time regime segmental orientation is enhanced, but stress is unchanged.[25] Therefore, we assume that in the linear viscoelastic response of polymer

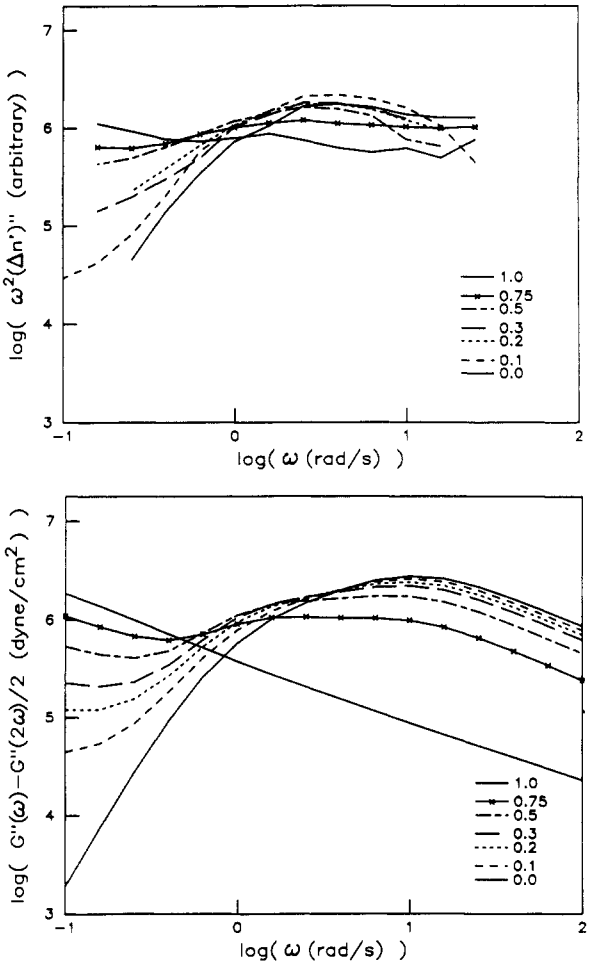

Figure 3. (a, Top) Measured frequency dependence of the imaginary part of the complex amplitude of the third normal stress difference using 1,3-birefringence. Curves shown connect the data points. (Reproduced from ref 15.) (b, Bottom) RHP model prediction for the imaginary part of the complex amplitude of the first normal stress difference on a scale appropriate for comparison with the optical measurements in (a).

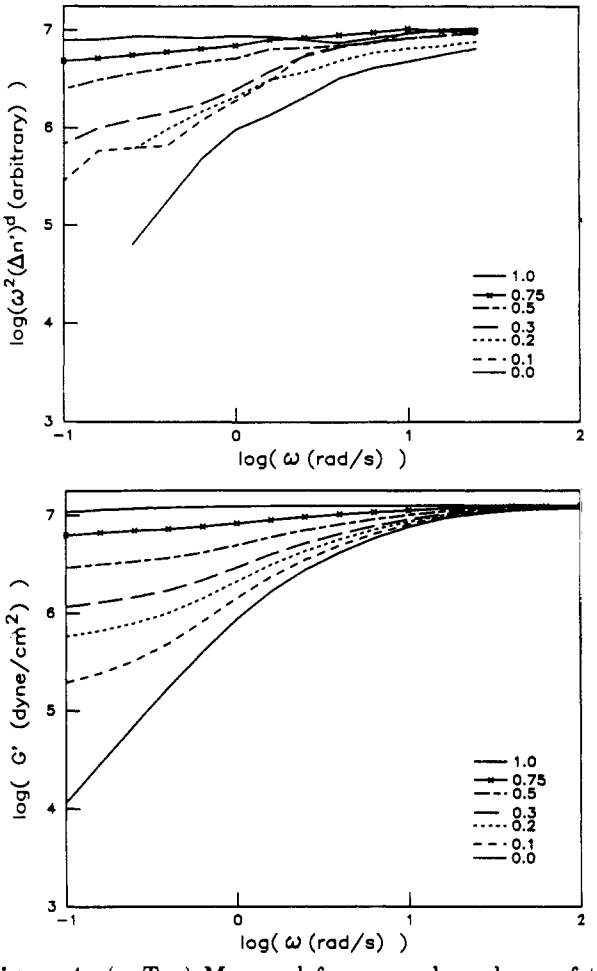

Figure 4. (a, Top) Measured frequency dependence of the displacement component of the third normal stress difference using 1,3-birefringence. Curves shown connect the data points. (Reproduced from ref 15.) (b, Bottom) Displacement component of the first normal stress difference predicted by the RHP model on a scale appropriate for comparison with the optical measurements in (a).

melts, this coupling enhances local segmental orientation but does not contribute to the stress. The dichroism results presented here measure local orientation (anisotropy in the orientation distribution of C–D bonds). Therefore the dichroism spectra are expected to contain two contributions: the classical rubberlike orientation (associated with elastic stress) and orientation driven by steric interaction with the anisotropic surrounding matrix. Two approaches to include the effect of local orientational coupling in melt viscoelasticity have been proposed[26,27] and will be discussed in section 5 when we compare the predictions of molecular theories to the results presented below.

4.1. Long-Chain Relaxation. The dichroism spectra record the frequency dependence of the orientation of the labeled chains, which can be compared with model predictions. They are presented in arbitrary units, scaled so that the plateau values of ω^2L' and ω^2S' at high frequency coincide with those of the model described in section 5. The results of dichroism measurements for long-chain labeled blends are shown in part a of Figures 5 and 6: the product of the real part of the complex amplitude L^* and the squared frequency, $-\omega^2L'$, is in Figure 5a, and the imaginary part, ω^2L'', is in Figure 6a. Part b of these figures again show the predictions of the model presented in the next section. Although the absolute magnitudes of the spectra are not known, the relative values for the different blends are the same on both Figures 5a and 6a.

All of the blends show a high-frequency plateau in $-\omega^2L'$, which relaxes toward low frequency. The amount of relaxation increases monotonically as Φ_L decreases from $\Phi_L = 1$ to 0.3, and remains unchanged for $\Phi_L \leq 0.3$. While the lowest frequency used in the dichroism measurements is more than an order of magnitude higher than ω_L, substantial long-chain relaxation is evident. The magnitude of the relaxation of $-\omega^2L'$ is, however, much smaller than that of $-\omega^2(\Delta n')'$ (Figure 2a), revealing the slower relaxation of the long chains relative to the blend as a whole.

The imaginary part of the complex coefficient of the long-chain dichroism (eq 4.1), ω^2L'', shows a transition with composition from the relatively flat, gradually decreasing curve characteristic of the pure long polymer and the $\Phi_L = 0.75$ blend, to the broadly peaked appearance for $\Phi_L = 0.5$–0.1. The relative magnitude of $-\omega^2L'$ and ω^2L'' can be seen by comparing Figures 5a and 6a. The magnitude of $-\omega^2L'$ generally decreases as Φ_L decreases; however, ω^2L'' in the vicinity of the peak frequency increases as Φ_L decreases. Roughly speaking, $-\omega^2L'$ and ω^2L'' are related to the elastic and dissipative response of the long chains, respectively. Thus the general trend in the long-chain dynamics with addition of short chains to the matrix is a decrease in the storagelike response and an increase in the losslike response as Φ_L decreases. This observation, occurring at frequencies much faster than the terminal loss of the long polymer, supports the idea of constraint release.

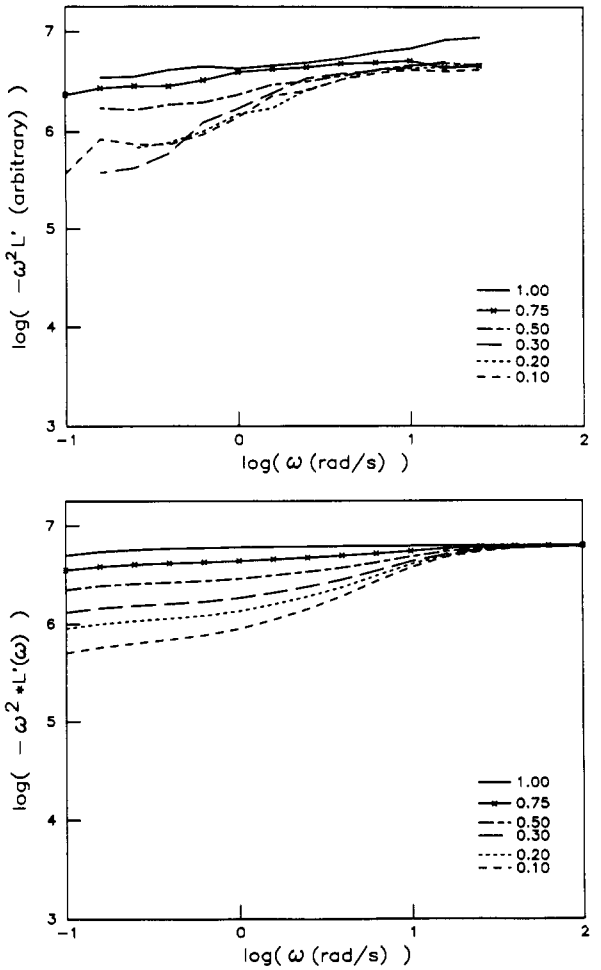

Figure 5. (a, Top) Measured frequency dependence of the real part of the complex amplitude of the long-chain response using 1,3-dichroism of blends with long chains labeled. Curves shown connect the data points. (b, Bottom) Predicted real part of the complex amplitude of the 1,3-dichroism (arbitrary units) with long chains labeled and an orientational coupling parameter ϵ = 0.3.

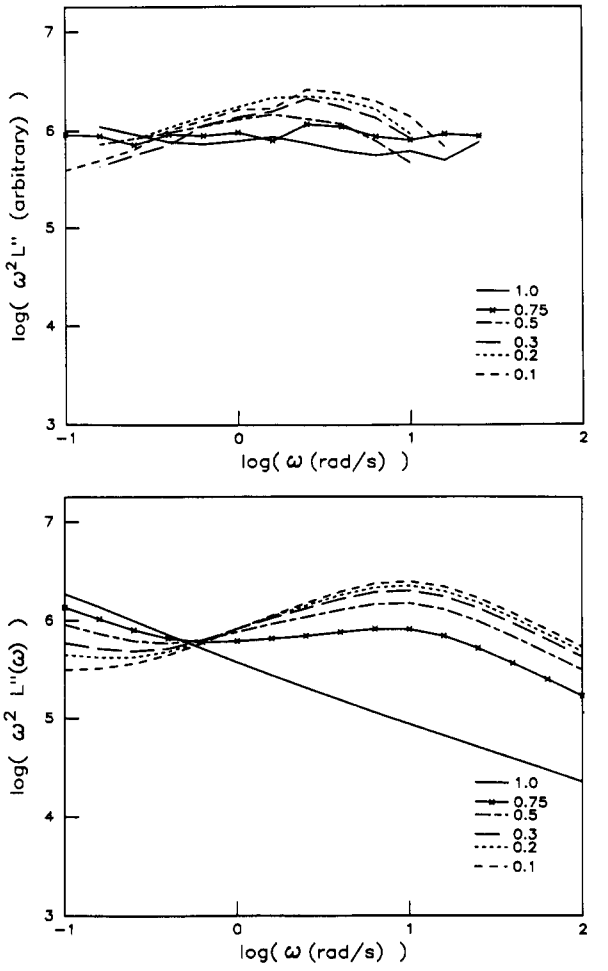

Figure 6. (a, Top) Measured frequency dependence of the imaginary part of the complex amplitude of the long-chain response using 1,3-dichroism of blends with long chains labeled. Curves shown connect the data points. (b, Bottom) Predicted imaginary part of the complex amplitude of the 1,3-dichroism (arbitrary units) with long chains labeled and an orientational coupling parameter ϵ = 0.3.

4.2. Short-Chain Relaxation. The dichroism measurements for short-chain labeled blends are presented in part a of Figure 7 and 8: Figure 7a, $-\omega^2 S'$; Figure 8a, $\omega^2 S''$. The logarithm of the absolute value of $-\omega^2 S'$ is shown in Figure 7a. For some compositions, $-\omega^2 S'$ takes on positive and negative values, as indicated in the legend. Like $-\omega^2(\Delta n')'$ and $-\omega^2 L'$, $-\omega^2 S'$ approaches a plateau at high frequency for all blends. The decrease from this plateau as frequency decreases is stronger than that of birefringence, $-\omega^2(\Delta n')'$ (Figure 2a), for each blend. All blends except $\Phi_L = 0.75$ show $-\omega^2 S'$ decreasing through zero and taking on negative values. The relaxation changes shape with composition, extending to lower frequency with increasing Φ_L, which can be seen clearly from the monotonic decrease in the frequency at which the sign change occurs as Φ_L is raised from 0.1 to 0.5.

The losslike component of the short-chain dichroism, $\omega^2 S''$, shows a broad peak much like that of $\omega^2(\Delta n')''$ (Figure 3a). For $\Phi_L = 0.1$ it is difficult to distinguish the $\omega^2 S''$ spectrum from that of $\omega^2(\Delta n')''$; however, as Φ_L increases, the peak in $\omega^2 S''$ shows a distinctly larger decrease on the low-frequency side than $\omega^2(\Delta n')''$. The general trend with increasing Φ_L is a decrease in the relaxation of $\omega^2 S''$ on the low-frequency side of the peak. The frequency of the maximum in the $\omega^2 S''$ peak is unchanged for Φ_L = 0–0.3. For Φ_L = 0.5 and 0.75 the peak has broadened so much that it is difficult to determine the frequency of the maximum.

The dichroism measurements of the short-chain relaxation, especially $-\omega^2 S'$, show a substantial dependence on the blend composition. This is in agreement with earlier results of step strain relaxation experiments on those blends that show short-chain dichroism relaxation persisting to much longer times in blends with high Φ_L than in the pure short-chain melt.[14] From these measurements alone, it is not possible to separate how much of the retardation is due to slowing of the rate of stress relaxation of the short chains and how much is due to orientational coupling between the short chains and the matrix containing unrelaxed long chains. From the perspective of testing molecular theories, the local orientational coupling is a complicating factor, which will be discussed in greater detail in the following section.

5. Comparison of Molecular Relaxations with Theory

In this section we compare the predictions of the Rubinstein–Helfand–Pearson modification of the reptation theory for bidisperse melts to the measured bulk viscoelasticity and component dynamics in oscillatory shear. The original reptation theory has been very successful in describing the viscoelastic behavior of monodisperse linear polymer melts;[6,28] however, the reptation model is deficient in describing polydisperse systems. This is due to the fact that a fundamental assumption of the reptation model is that the mean field of entanglements is relatively static

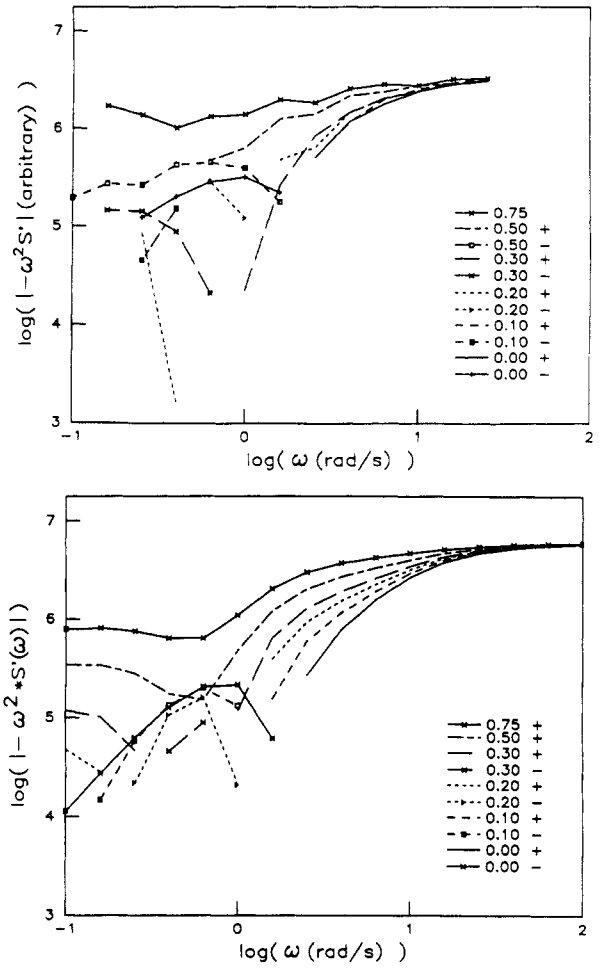

Figure 7. (a, Top) Measured frequency dependence of the real part of the complex amplitude of the short-chain response using 1,3-dichroism of blends with short chains labeled. For blends in which $-\omega^2 S'$ changes sign, two curves are shown, with the positive and negative segments indicated in the legend. (b, Bottom) Predicted real part of the complex amplitude of the 1,3-dichroism (arbitrary units) with short chains labeled and an orientational coupling parameter $\epsilon = 0.3$.

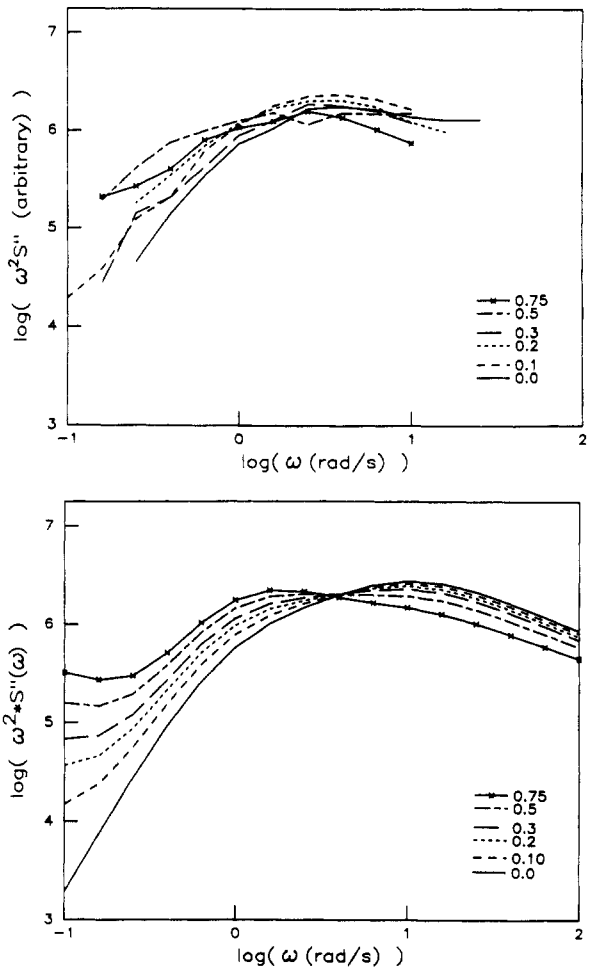

Figure 8. (a, Top) Measured frequency dependence of the imaginary part of the complex amplitude of the short-chain response using 1,3-dichroism of blends with short chains labeled. Curves shown connect the data points. (b, Bottom) Predicted imaginary part of the complex amplitude of the 1,3-dichroism (arbitrary units) with short chains labeled and an orientational coupling parameter $\epsilon = 0.3$.

on the time scale of reptation. Therefore, any relaxation mechanisms afforded a given chain due to the motion of chains in the surroundings are neglected. A consequence of this assumption is that the relaxation of a given chain in a polydisperse homopolymer melt is predicted to be a function only of its length, independent of the molecular weight distribution of the melt. This leads directly to a linear blending law for the viscoelastic properties. It has been known for many years[1,2,29] that this type of blending law does not correctly describe the relaxation spectrum of polydisperse melts.

Well-designed and carefully conducted experiments on bidisperse melts clearly show that the slow relaxation associated with the long polymer increases much less strongly than linearly with Φ_L, while the fast relaxation, on time scales characteristic of the short polymer, decreases hardly at all as Φ_L increases at low Φ_L. It was postulated[4] that as the short-chain volume fraction decreases a portion of the fast time relaxation is supported by the long polymer. The short-time relaxation mechanism of the long chains is thought to be afforded by the release of constraints imposed by short chains in the matrix.

Various models that improve upon the reptation theory by including the effect of "constraint release" or "tube renewal" have been proposed.[7-12] We do not undertake a comparison among these models here, but the interested reader is referred to the paper by Rubinstein and Colby.[10]

We have chosen to limit our discussion to the Rubinstein–Helfand–Pearson (RHP) model because it contains the essential features of the constraint release idea while using a minimum number of parameters. More general models that include the effect of "tube enlargement"[8,9] are not needed because for the molecular weights of the polymers used in this work $(M_S^3/M_e^2 M_L) \gg 1$.[14]

5.1. The Rubinstein–Helfand–Pearson Model. In the RHP model, it is assumed that the stress arises from the orientation of the statistical segments (of molar mass $\approx M_e$) of each chain. Two mechanisms of orientational relaxation are included: reptation and constraint release. The two mechanisms are assumed to be independent.

Reptation[5] consists of curvilinear diffusion of the molecule with concommitant stress relaxation as old, oriented constraints are escaped, and new, relaxed, tubelike regions are explored. The time dependence of this process is obtained from an analysis of a one-dimensional first passage time problem.[30] The fraction of the initial tube remaining at time t, μ, is given by

$$\mu(t/\tau) = \frac{8}{\pi^2} \sum_{\text{odd } p} \frac{1}{p^2} \exp(-p^2 t/\tau) \qquad (5.1)$$

where the relaxation time τ is the reptation time associated with complete departure from the tube, which varies as the third power of the molecular weight.[31]

In the original reptation model this is the only mechanism for relaxation. Relaxation due to motion of the

surrounding molecular constraints is neglected. This is clearly not a good assumption for polydisperse systems. Since the reptation time varies as a high power of molecular weight, high molecular weight chains require a longer time to escape all of their initial constraints than the characteristic lifetime of matrix constraints. Thus, the fundamental picture in reptation-based constraint release models is that the tube is vacated by curvilinear diffusion and the orientation of the remaining tube is destroyed by constraint release. Assuming that the two mechanisms are independent, the net orientation of the chain can be expressed as the product of the fraction of tube remaining, μ, and the relative orientation of the present tube compared to the initial tube, R

$$F_K(t) = R(t)\mu(t/\tau_K) \tag{5.2}$$

where F is the relaxing memory function of a test chain and subscript K refers to the length of the test chain. The dependence of the relaxation of the K chain on the matrix molecular weight distribution is described by $R(t)$.

The assumption that reptation and constraint release are independent has been questioned by Watanabe and Tirrell, and they have presented an alternate model in which the two processes are coupled.[11] A further complication arises if the diameter of the tubelike region occupied by the test chain increases because constraints are disappearing faster than the time required for a point on the test chain to diffuse the distance between constraints.[8-10] Doi et al. have argued that this will *not* be the case if[32]

$$\frac{M_S^3}{M_e^2 M_L} \gg 1 \tag{5.3}$$

Diffusion results suggest that this criterion is satisfied when the ratio in eq 5.3 is greater than 10.[33] In the present experiments, $M_S^3/(M_e^2 M_L) = 124$; therefore, it is reasonable to apply a model where the tube diameter is assumed to be constant.

Relaxation due to constraint release is assumed to occur by conformational rearrangement by a random hopping of chain segments as in the Verdier–Stockmayer model.[34] Orwoll and Stockmayer[35] have shown that the relaxation spectrum of this chain is equivalent to that of the Rouse model.[36] The distinctive feature of the RHP model is that the hopping time, τ_w, of a segment is proportional to the reptation time of the chains that impose the constraint; the fraction of chain segments having a hopping time $\tau_{w,K}$ is equal to the volume fraction of K chains, Φ_K. Hence, for a binary blend $R(t)$ is equal to

$$R(t) = \Phi_L\Theta(t/\tau_L) + \Phi_S\Theta(t/\tau_S) \tag{5.4}$$

where Φ_L and Φ_S are the volume fractions of long and short chains. The value of Θ is given by the normalized Rouse relaxation function

$$\Theta(t/\tau_w) = \frac{1}{N}\sum_{j=1}^{N} e^{-2t/\tau_j} \tag{5.5}$$

where $\tau_j = \tau_w/4\sin^2(\pi j/2(N+1))$, τ_w is the characteristic waiting time for a constraint release event, and N is the number of Rouse modes or the number of springs in the bead–spring model. It is reasonable to assume that the two hopping times, $\tau_{w,L}$ and $\tau_{w,S}$, are related to the reptation times of the two components by

$$\tau_{w,K} = \kappa\tau_K \tag{5.6}$$

where $K = L$ or S and where κ is an order one constant.[6-12] In the following discussion we take $\kappa \equiv 1$ and replace $\tau_{w,K}$ with τ_K. (Alternatively, κ could be treated as an adjustable parameter. We comment on this at the end of section 5.4.1.)

The relaxation modulus for the RHP model is given by

$$G(t) = G_N^0[\Phi_L F_L(t) + \Phi_S F_S(t)] \tag{5.7}$$

where F_K is given by eq 5.2 and $R(t)$ is given by eq 5.4 and an approximate form for $\Theta_S(t/\tau_w)$ given in eq A.1 of Appendix 1. There are two parameters in the model, G_N^0 and τ_S, which are readily determined from linear viscoelastic data on the monodisperse short polymer. Data for the molecular weights of the two species are used to fix the long-chain relaxation time according to the theoretical scaling relationship

$$\tau_L = (M_L/M_S)^3\tau_S \tag{5.8}$$

The dynamic modulus predicted by the model is computed from the relationship

$$G^*(\omega) = i\omega\int_0^\infty dt\, G(t)e^{-i\omega t} \tag{5.9}$$

Hence, from eq 5.7

$$G^*(\omega) = G_N^0[\Phi_L F_L^* + \Phi_S F_S^*] \tag{5.10}$$

where, from eqs 5.2 and 5.4

$$F^*_K = i\omega\int_0^\infty dt\, R(t)\mu(t/\tau_K)e^{-i\omega t} \tag{5.11}$$

The model predicts not only the bulk viscoelastic response (eq 5.10) but also the contribution to the dynamic modulus of each molecular weight component (eq 5.11).

In this paper we wish to compare the model predictions with the following measured variables; the linear viscoelastic shear moduli and the dynamic birefringence and dichroism both measured in the 1,3-plane. The latter quantities require a finite strain constitutive equation to relate them to linear viscoelastic properties. To do this we make use of the generalized equation of linear viscoelasticity, which predicts the relations given in eqs 3.11–3.14. With this model, the contributions of long and short components, $K = L$ or S, to the first normal stress are given by

$$-\omega^2\Psi_{1,K}' = G_N^0\left[F_K'(\omega) - \frac{1}{2}F_K'(2\omega)\right] \tag{5.12}$$

$$\omega^2\Psi_{1,K}'' = G_N^0\left[F_K''(\omega) - \frac{1}{2}F_K''(2\omega)\right] \tag{5.13}$$

$$\omega^2\Psi_1^{\,d} = G_N^0 F_K'(\omega) \tag{5.14}$$

Their contribution to the third normal stress difference is simply proportional to these values as implied by eq 3.14.

The viscoelastic properties and the birefringence can be compared directly with the predictions of this model. However, the dichroism from labeled chains measures anisotropy in the orientation distribution of carbon–deuterium bonds, which may not be directly proportional to the labeled chains' contribution to the stress. Before we present the model predictions and compare them with the experimental results, we must first discuss the relationship between the dichroism from labeled components and their contribution to the stress.

5.2. The Effect of Short-Range Orientational Coupling. Numerous experiments have demonstrated that short-range coupling exists between free probe molecules and oriented macromolecules in a polymer matrix. These include studies which show that small penetrant molecules in extended polymer networks obtain

a steady-state anisotropic orientation distribution proportional to that of the network segments.[19-21,24] Additional experiments in homopolymer systems show that oligomers attain a steady-state orientation when the surrounding network is oriented.[22,23] Finally, experimental results on bidisperse polymer melts show that the short chains in the melt retain some orientation so long as the matrix as a whole is oriented.[14,37] Such an orientational cooperativity has been attributed to steric interaction between chains, and modifications of the classical theory of rubber elasticity to include this effect have been developed.[25,38,39]

The effect of short-range orientational coupling on polymer melt rheology has been modeled in two ways.[26,27] The fundamental difference between the theories is that in the Merrill and Tirrell model[27] the orientation of the matrix is coupled only to the relaxed ends of the chain that have emerged from the original tube, while in the Doi et al. model[26] the orientation of the matrix is coupled to the chain all along its contour. The two models produce different predictions regarding the shape of the orientational relaxation spectrum; however, a detailed comparison between them has not been made.

In this work we choose the latter model because it is more consistent with the earlier theory of Jarry and Monnerie for orientational coupling in rubber, which assumes that molecular packing constraints apply to every segment along each chain.[25] Accordingly, the orientation of the chain consists of two parts that are additive: (i) orientation at the statistical-segment level imparted by the applied strain and (ii) additional orientation at the monomer level driven by interaction with the matrix.[14,26]

$$n_{ij}''_K = C'(\lambda)\left[\left\langle r_i r_j - \frac{1}{3}r^2\delta_{ij}\right\rangle_K + \frac{\epsilon}{1-\epsilon}\left\langle r_i r_j - \frac{1}{3}r^2\delta_{ij}\right\rangle\right] \tag{5.15}$$

where $C'(\lambda)$ is the optical coefficient of proportionality between the imaginary part of the refractive index tensor and the order parameter tensor in square brackets, λ is the wavelength of light, $\langle r_i r_j - {}^1/_3 r^2\delta_{ij}\rangle$ is the order parameter tensor for segments of molecular weight M_e (the angle brackets alone denote an average over all chains; the brackets with subscript K denote an average over the K chains [$K = L$ or S]), and ϵ is the coupling parameter that describes the strength of the short-range orientational coupling.

The parameter ϵ is a temperature-dependent material property of the bulk polymer. The first term on the right-hand side of eq 5.15 corresponds to the contribution of the K chains to the elastic stress according to the classic theory of rubber elasticity. This term is proportional to that given by eq 5.11. The second term on the right-hand side of eq 5.15 is proportional to the orientation of the matrix as a whole, which is given by eq 5.10. With a knowledge of the value of the coupling parameter, ϵ, the frequency dependence of the dichroism can be predicted from the RHP model using eq 5.15 together with eqs 5.10 and 5.11. For the hydrogenated polyisoprenes used in this study, the value of ϵ can be estimated from our step strain relaxation experiments,[14,37] which indicate ϵ is between 0.30 and 0.45.

5.3. Model Predictions for Shear and Normal Stress. 5.3.1. Dynamic Modulus. The experimental dynamic shear moduli and the theoretical predictions of the RHP model are shown in Figure 9. The storage moduli (Figure 9a) for all blends have the same high-frequency plateau. With decreasing frequency the storage modulus is initially constant and then enters a strong relaxation. For the two monodisperse polymers, this terminal relaxation consists of a fairly sharp transition into the terminal

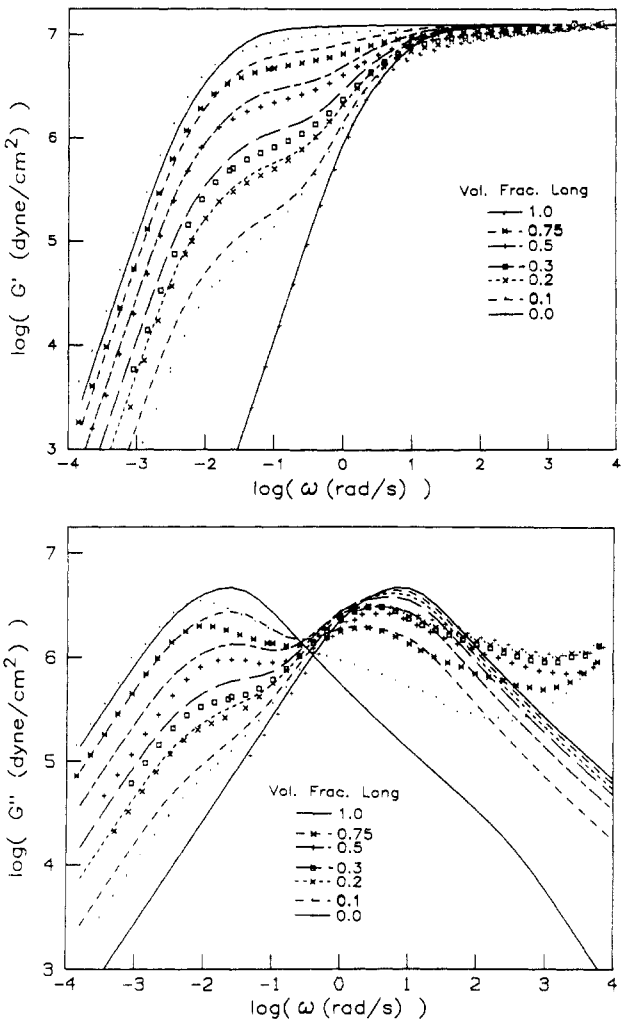

Figure 9. (a, Top) Comparison of RHP model predictions (curves) and measurements (points) for the storage modulus of binary blends. (b, Bottom) Comparison of RHP model predictions (curves) and measurements (points) for the loss modulus of binary blends.

region where G' decreases as ω^2. For the blends there is an inflection in the relaxation: the storage modulus of the blends begins to drop near the frequency where the pure short component enters its terminal relaxation, but then with decreasing ω the rate of decay slows $G'(\omega)$ and has an inflection point that in some cases appears as a second plateau ($\Phi_L = 0.5$ and 0.75). The terminal relaxation of the blends is reached at a frequency close to that of the pure long polymer. The shape of the theoretical storage modulus at low frequency ($\omega < 0.01$ rad/s) is similar for all of the blends but has a magnitude that is Φ_L^2 times that of the pure long polymer.

A qualitative comparison of model predictions and experimental results shows that there is a general agreement between the two families of curves. After fixing the short-chain relaxation time, the shape of the two pure component curves and the position of the long-chain curve are approximately correct. The relative magnitude of G' at low frequency for the blends compared with that of the pure long polymer falls with Φ_L very nearly as predicted. The experimental results have a broader relaxation spectrum than the theoretical results. For the blends this manifests itself in a sharper inflection in the theoretical G' than in the actual one at intermediate frequencies, $\omega_S < \omega < \omega_L$.

The predicted and measured loss moduli are shown in Figure 9b. The loss peaks for the pure components are predicted to be almost symmetrical, falling off with a slope

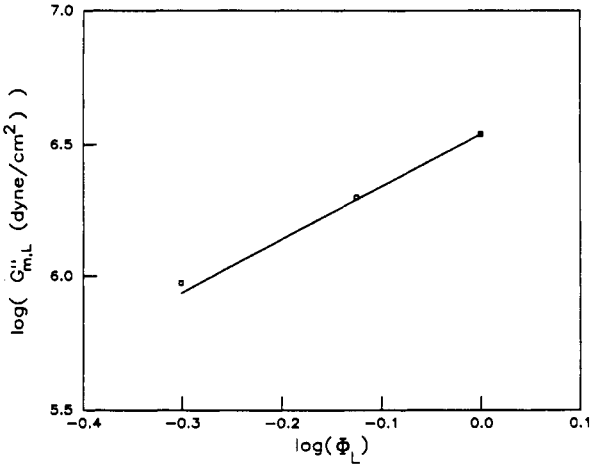

Figure 10. Magnitude of the low-frequency loss peak as a function of composition. Point markerrs shown the maximum value of G'' on the low-frequency peak. The solid line shows a power law with an exponent of 2.

of +1 on the low-frequency side and −0.64 on the high-frequency side. Depending on the long-chain volume fraction, the blends have peaks at high frequency, low frequency, or both. As Φ_L increases from zero, the magnitude of the high-frequency peak decreases slightly, followed by a larger decrease as Φ_L approaches 1. Based on data between $\Phi_L = 0.5$ and 1, the magnitude of the loss modulus near the low-frequency loss peak falls as Φ_L^2. Comparison between theory and experiment for both of these peaks is shown in Figures 10 and 11.

Although the RHP model and the experimental loss moduli data are qualitatively similar, there is a clear discrepancy between the actual and predicted shapes, especially at high frequencies. This is mainly due to the neglect of loss processes in the transition region[28] that are clearly seen to be important on the right-hand side of Figure 9b. None of the models referenced above include such processes. This same deficiency is evident in the discrepancy between the high-frequency behavior of the observed and predicted storage moduli.

5.3.2. Normal Stress Difference. The components of the predicted first normal stress difference in oscillatory flow are shown in part b of Figures 2–4: the real part of $\omega^2\Psi_1^*$ is shown in Figure 2b, the imaginary part in Figure 3b, and the displacement component in Figure 4b. These are calculated from the RHP model prediction by applying the generalized linear viscoelastic constitutive equation. The predicted real part, $-\omega^2\Psi_1'$, (Figure 2b) may be compared with the measured frequency dependence of $-\omega^2(\Delta n')'$ (Figure 2a), by assuming that the third normal stress difference is proportional to the first. The model correctly predicts that at high frequency $-\omega^2\Psi_1'$ approaches a plateau and that it decreases with decreasing frequency. It also correctly predicts that $-\omega^2\Psi_1'$ changes sign from positive to negative only for $\Phi_L = 0$ and 0.1 and predicts the frequency at which this occurs. The shape of the spectra for $\Phi_L = 0.3$, 0.5, and 0.75 shows good agreement between the model and the measured results. (The discrepancy between the prediction and measurement for $\Phi_L = 1$ is actually within the uncertainty in the birefringence measurement for the pure long polymer, due to experimental difficulties encountered with very stiff samples.) For the blends with $\Phi_L = 0.1$ and 0.2, the measured spectra decrease more strongly than the model predicts.

The RHP model predictions for $\omega^2\Psi_1''$ are shown in Figure 3b. The range of frequencies in the figure is above the long-chain loss peak, and it is again evident that in this region the losses in the model are too small. For

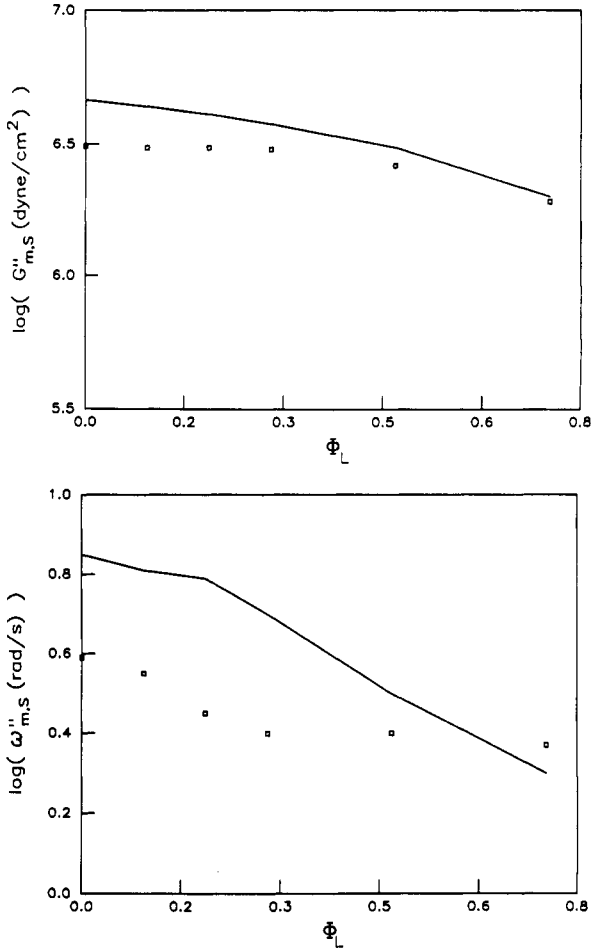

Figure 11. (a, Top) Magnitude of the high-frequency loss peak as a function of composition. Data points are experimental values of the maximum of G'' for the high-frequency peak. The solid line shows the prediction of the RHP model. (b, Bottom) Position of the high-frequency loss peak as a function of composition. The point markers show the frequency at the maximum in G'' at high frequency. The solid line shows the prediction of the RHP model.

example, there is a large discrepancy between the shape of $\omega^2(\Delta n')''$ (Figure 3a) and the predicted $\omega^2\Psi_1''$ in the case $\Phi_L = 1$. For $\Phi_L = 0.75$, the model has a broad peak at high frequency. This peak becomes larger and narrower as Φ_L decreases. The observed birefringence shows the same trend. At the low end of the frequency range considered here, the predicted $\omega^2\Psi_1''$ for all of the blends stops decreasing or even starts increasing with decreasing frequency. Only the pure short polymer is predicted to have a monotonic relaxation. This prediction also agrees with the birefringence result.

Figure 4b shows the predicted displacement component, $\omega^2\Psi_1^d$. All of the melts have a common high-frequency plateau. With decreasing frequency, $\omega^2\Psi_1^d$ decreases: for pure short polymer the decrease is strong, but as Φ_L increases the decrease becomes smaller, until for pure long polymer, $\omega^2\Psi_1^d$ is almost contant over this frequency range. This trend is in agreement with the birefringence results, $\omega^2(\Delta n')^d$ (Figure 4a).

The discussion so far has been limited to comparing the RHP model to the shear stress and optically measured normal stress difference. Using only two parameters, the plateau modulus, G_N^0, and the short-chain relaxation time, τ_S, the model provides a successful prediction of the relaxation spectra, although it is deficient at high frequencies. In what follows, we will show that further insight into the relaxation processes can be obtained by using optical measurements and selective labeling to observe

the orientation of the long and short components individually.

5.4. Model Predictions for the Long and Short Components. The RHP model predictions for the 1,3-dichroism with either long or short chains labeled are given by

$$(\Delta n'')^*_K = c''[\Psi^*_{1,K} + a_{NE}\Psi^*_1]/(1 + a_{NE}) \quad (5.16)$$

where c'' is an unknown coefficient equal to the product of the stress optical coefficient for dichroism and the ratio of the third and first normal stresses, $a_{NE} = \epsilon/(1-\epsilon)$ is the coefficient arising from short-range orientational coupling (see eq 5.15), and K is either L or S. The notation for the component dichroism is the same as in section 4: the letters L and S represent $\Delta n''_L$ and $\Delta n''_S$, respectively. We have arbitrarily set the value of $c'' = 1$. Based on our previous studies, we believe ϵ to be on the range of $\epsilon = 0.30$–0.45 for deuterated polyisoprene. We have chosen $\epsilon = 0.3$ for comparison with experiment. Predictions of the model with $\epsilon = 0$ are presented in Appendix 2 and compared with those shown below. Model predictions for $\epsilon = 0.4$ can be found in ref 40.

5.4.1. Long-Chain Response. The predictions for the dichroism spectra of the long polymer are shown in part b of Figures 5 and 6. The real part of $-\omega^2L^*$, $-\omega^2L'$, is shown in Figure 5b. The curves start from the same high-frequency plateau and decay as frequency is lowered. For the pure long chains, very little relaxation occurs over this frequency range; the amount of relaxation increases as short chains are added, to the point that for $\Phi_L = 0.1$ the long-chain contribution to the stress relaxes almost a full order of magnitude in this frequency range (see Figure 12 in Appendix 2) and the long-chain dichroism falls to one-tenth its plateau value on this range. The corresponding dichroism results for the long-chain orientation are shown in Figure 5a. The data are scaled so that the high-frequency values for all of the blends coincide. As Φ_L decreases the rate of relaxation increases, in qualitative agreement with the RHP model. However, relaxation in the model begins at approximately 0.5 decades higher frequency than the experimental data.

The predicted imaginary part of the complex amplitude of the long-chain dichroism times the squared frequency, ω^2L'', is shown in Figure 6b. A qualitative change in the ω^2L'' spectrum occurs between $\Phi_L = 1$ and 0.75: a peak appears when the blend contains 25% by volume of short polymer, and it has the same peak frequency as the peak in the pure short-chain $\omega^2(\Delta n')''$ spectrum (see Figure 3). The magnitude of this high-frequency peak increases as Φ_L decreases. These predicted ω^2L'' spectra may be compared with the experimental results in Figure 6a. The scaling of the spectra in Figure 6a is the same as in Figure 5a. Consistent with the model prediction, a peak appears on the long-chain spectrum and its magnitude increases monotonically as Φ_L decreases. The peak frequency of the experimental data is about 0.5 decades lower than in the model. This agrees with the ω^2L' results and suggests that the appropriate constraint release time may be as much as three times the relaxation time of the S chains.

5.4.2. Short-Chain Response. The theoretical predictions for the short chains are shown in part b of Figures 7 and 8. Figure 7 shows the real part of $-\omega^2S^*$. Starting from a high-frequency plateau, the theoretical $-\omega^2S'$ decays with decreasing frequency and, at volume fractions less than $\Phi_L = 0.5$, it also changes sign at low frequencies (Figure 7b).

Comparing this with the experimental data in Figure 7a indicates that the RHP model *with short-range coupling* is in qualitative agreement with the experimental results. The lack of a sign change in $-\omega^2S'$ for $\Phi_L = 0.75$ and a double sign change for $\Phi_L = 0.2$ are found in both the theoretical and experimental curves.

The imaginary part of ω^2S^* is shown in Figure 8. In this frequency range the prediction of the RHP model is that ω^2S^* should have a broad peak that shifts to lower frequency as the concentration of long polymer increases. The shift can be substantial. For short chains in a blend with 75% volume long polymer, the peak in the predicted ω^2S'' occurs 0.8 decades below the peak in the pure short-polymer spectrum.

Experimentally, the peak in ω^2S'' changes very little. The shape changes only slightly as Φ_L increases from 0 to 0.3. The curves at $\Phi_L = 0.5$ and 0.75 have stronger low-frequency shoulders than the others, but their peaks have not shifted as predicted by the model. Also notice that the peak frequency in ω^2S'' (Figure 8a) is the same as in ω^2L'' (Figure 6a) but is 0.5 decades below the peak of the calculated curves (Figure 8b). Physically, the dichroism results show that when the high-frequency loss peak is of constant magnitude ($\Phi_L < 0.5$), the constraint release contribution to the short-chain relaxation remains essentially unchanged.

6. Discussion

Using dynamic infrared dichroism with deuterium labeling of the individual components of a bidisperse melt, we have been able to measure the response of the long- and short-chain species independently in oscillatory shear experiments. The results were compared with predictions from the RHP model, pointing out both its strengths and limitations. It is clear that the high-frequency loss appearing in the long-chain response is at the same frequency as the short-chain loss. This supports the validity of the fundamental idea of constraint release. From our results we cannot rule out the possibility that the short-chain stress relaxation may be strongly retarded by addition of long chains to the melt. However, it is in these small-strain experiments that the characteristic relaxation mechanisms of the short chains should not be greatly perturbed. This agrees with the finding that the diffusion of a fully entangled short polymer is independent of matrix composition.[33] However, it is expected that orientational relaxation of the short chains is retarded. This can be explained in terms of a short-range orientational coupling, which has been found in a wide range of other experiments. When this is taken into account, the model predictions are in qualitative agreement with the both the short-chain and long-chain results.

In the present model calculations, all of the parameters are fixed by the theory or by well-defined measurements: G_N^0 is the plateau modulus taken from the relaxation modulus of the pure long polymer, τ_S is the reptation time of the pure short polymer and is also determined from $G(t)$ of the short polymer, and ϵ is the orientational coupling coefficient determined from earlier step strain relaxation measurements of the dichroism of the low molecular weight component of binary blends.[14,37] The long-chain reptation time τ_L is fixed by the molecular weight scaling law predicted by the reptation theory and the experimental value of τ_S. The ratio of the constraint-release waiting time due to K chains to the reptation time of K chains, κ, was set equal to one.

The most significant discrepancy between the model and the experiments is that the relaxation spectra for both the long and the short polymers over the frequency range covered in the optical experiments are essentially composition independent for $\Phi_L < 0.5$. It is significant that over this range of composition the high-frequency loss

peak of the bulk is also composition independent. Since constraint release is governed by the mean field of chains surrounding a given chain, it is not unreasonable that the behavior of the constraint release function $R(t)$ in the frequency range of the high-frequency loss should also be independent of composition in this regime. The RHP model does not capture this characteristic. It is worth noting, however, that the apparent discrepancy between the model and the experiments would be reduced if the constraint release time was taken to be three times the reptation time ($\kappa = 3$ in eq 5.6), as suggested by the long-chain dichroism results. We have not attempted any further comparison with the RHP model using this value, because a more complete theory of the high-frequency transition zone is needed to substantially improve the agreement between theory and experiment in this frequency range.

Acknowledgment. We are grateful for support for this research from the National Science Foundation through the Presidential Young Investigator (G. Fuller) and Graduate Fellowship (J. Kornfield) programs and from the Exxon Foundation and the Center for Materials Research at Stanford University. We thank Lewis Fetters for synthesizing the polymers employed in this study. We would like to thank Ron Larson for reading the manuscript and for his helpful comments and suggestions.

Appendix 1: Matrix Relaxation Spectrum Used in RHP Model Calculations

The physical ideas of the Rubinstein–Helfand–Pearson model are explained in section 5. In this appendix, we describe the approximate form of the Rouse spectrum that is used for the calculations presented in section 6. We choose an approximate form for the series expression in eq 5.5 to eliminate the parameter N, the number of Rouse segments, because the relaxation of the real chain must be independent of the exact number of segments we use to model it. Indeed, the Rouse spectrum is insensitive to the exact value of N once the number of segments is large. A function that approximates the Rouse spectrum well for time t short relative to the longest Rouse relaxation time is[10]

$$\theta(t/\tau_w) \approx \exp(-4t/\tau_w) I_0(4t/\tau_w), \quad t \ll N^2\tau_w/\pi^2 \tag{A.1}$$

where τ_w is the waiting time for the Rouse-like conformational rearrangement (see section 5) and I_0 is the modified Bessel function of zero order. This function is used to describe the slow and fast modes of constraint-release (CR) relaxation (see eq 5.4): the waiting time for CR due to the motion of short chains is taken to be approximately τ_S, the reptation time of a short chain, and similarly the waiting time for long-chain CR is taken to be τ_L.

Use of the approximate spectrum is valid if we are concerned only with $t \ll N^2\tau_w/\pi^2$. In the model, each chain relaxes by reptation and CR, and in no case does complete relaxation take longer than the time required for the chain to renew its conformation by reptation alone. Therefore, for a short chain we are concerned with $t < \tau_S$ and for a long chain $t < \tau_L$. Expression A.1 is valid for the short chains because τ_S is short relative to the faster of the terminal Rouse relaxation times, $\tau_{1,S}$, given by

$$\tau_{1,S} = \frac{N_S^2\tau_S}{\pi^2} \tag{A.2}$$

Regardless of the exact value of N_S, it should be on the order of magnitude of M_S/M_e, which is approximately 29 for the short polymer used in this study. Thus, the approximate Rouse spectrum above is appropriate for describing both fast and slow CR relaxation of the short polymer.

In the case of a long chain, the same argument leads to the conclusion that the approximate form for the slow CR relaxation, with a terminal Rouse relaxation time $\tau_{1,L} = N_L^2\tau_L/\pi^2$, is appropriate, since $\tau_L \ll \tau_{1,L}$. However, the fast CR relaxation has a terminal time $\tau_{1,S}$ that is not necessarily long compared with τ_L, the longest time of interest. The relationship between $\tau_{1,S}$ and the reptation time for long polymer is

$$\tau_{1,S} = \frac{N_S^5\tau_L}{N_L^3\pi^2} \tag{A.3}$$

For the polymers used in this study, $N_L/N_S \approx 7$, which gives $\tau_{1,S} \approx 0.25\tau_L$. Since the longest relaxation time for fast CR is smaller than long-chain reptation time, the cross-term in the calculation of the long-chain relaxation F_L (see eq 5.11) that decays as $\mu(t/\tau_L)\theta(t/\tau_S)$ will differ in our calculations from the result that would be obtained if the true Rouse spectrum were used for θ. The short-chain CR gives rise to the fast mode of relaxation of the long polymer; the use of the approximate spectrum, therefore, may alter the shape on the low-frequency side of the high-frequency peak in the long-chain losslike response. Since this does not change the main features of the model predictions, the same form of $R(t)$ (eq 5.4) with $\theta(t/\tau_w)$ given by the approximate expression in eq A.1 was used for both the long and short chains.

For convenience of readers who may wish to reproduce the model calculations, we close this appendix with a few details pertaining to the numerical evaluation of F^*_j given in eq 5.11. Replacing $R(t)$ with expression 5.4 gives

$$F^*_j = \Phi_L i\omega \int_0^\infty dt\, \theta(t/\tau_L)\mu(t/\tau_j)e^{-i\omega t} + \Phi_S i\omega \int_0^\infty dt\, \theta(t/\tau_S)\mu(t/\tau_j)e^{-i\omega t} \tag{A.4}$$

The integrands in eq A.4 may be expanded in terms of the reptation relaxation function (eq 5.1) and the approximate Rouse relaxation function (eq A.1):

$$\int_0^\infty dt\, \theta(t/\tau_k)\mu(t/\tau_j)e^{-i\omega t} = \frac{8}{\pi^2}\sum_{\text{odd } p}\frac{1}{p^2}\int_0^\infty dt\, I_0(4t/\tau_k)e^{-\alpha_{pjk}t} \tag{A.5}$$

where $\alpha_{pjk} = p^2/\tau_j + 4/\tau_k + i\omega t$. The integrals in the series in eq A.5 may be evaluated as follows

$$\int_0^\infty dt\, I_0(4t/\tau_k)e^{-\alpha_{pjk}t} = \frac{1}{(\alpha_{pjk}^2 - (4/\tau_k)^2)^{1/2}} \tag{A.6}$$

The functions $F^*_j(\omega)$ were evaluated numerically by computing the partial sums of the series in eq A.5 until the last term is less than 10^{-8} of the current sum.

Appendix 2: Comparison of Model with and without Orientational Coupling

In the body of the paper (section 5.4), predictions for the frequency dependence of the dichorism of each molecular weight component in the bidisperse melt are presented based on the RHP model modified to include intermolecular orientational coupling. Experimental observations, which indicate that this is appropriate, are described in section 5.2, including results that indicate that the value of the coupling parameter ϵ is slightly greater than or equal to 0.3 for the polymers used in the present study. Therefore, the measured dichroism spectra are

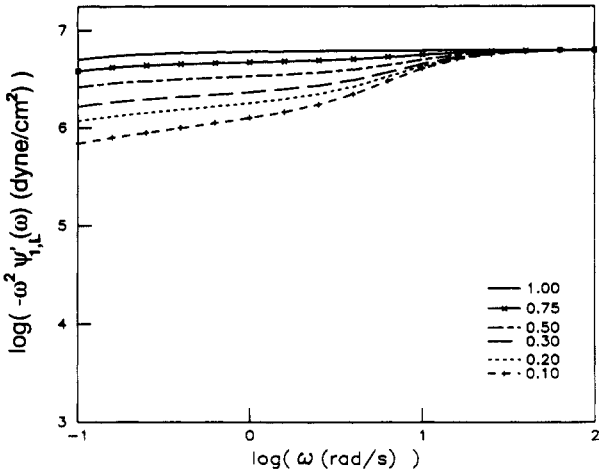

Figure 12. Predicted contribution of the long chains to the real part of the complex amplitude of the first normal stress difference.

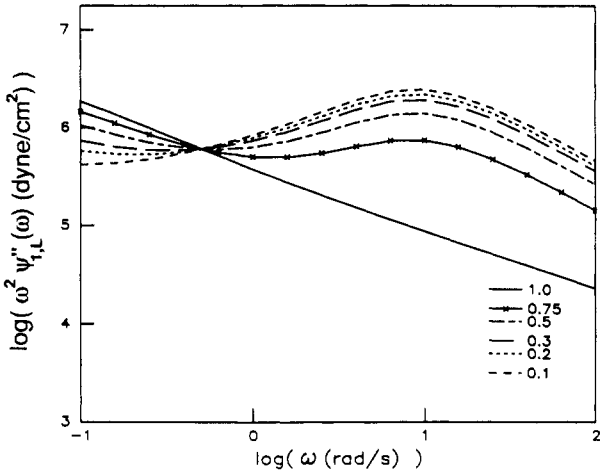

Figure 13. Predicted contribution of the long chains to the imaginary part of the complex amplitude of the first normal stress difference.

compared with predicted spectra of the modified RHP model with $\epsilon = 0.3$. For the benefit of those interested in the influence of orientational coupling, we present in this appendix the spectra predicted by the unmodified RHP model (i.e., $\epsilon = 0$).

The physical significance of the spectra presented here is that they show the dynamic response of the orientation distribution of statistical segments of the chain (on a more coarse-grained scale than the C–D bond orientation distribution probed by infrared dichroism). It is the restoring force along statistical segments that gives rise to the stress according to the model. Thus, the spectra presented below can be viewed as the frequency dependence of the contribution of each component to the stress. In the absence of intermolecular orientational coupling, the frequency dependence of the infrared dichroism spectra is identical with that of the contribtuion of the labeled chains to the stress. When short-range coupling is included in the model, the infrared dichroism (bond-level orientation distribution) spectra are altered, but the underlying contribution to the stress is not.

The long-chain contributions to the complex amplitude of the first normal stress difference, $-\omega^2\Psi'_{1,L}$ and $\omega^2\Psi''_{1,L}$ (see eqs 5.12 and 5.13), are shown in Figures 12 and 13, respectively. The former is related to the storagelike response of the long chains and the latter to the dissipative response. As discussed in the body of the paper, the frequency range of these plots spans the loss peak of the short polymer and is in the rubbery plateau, well above the loss peak of the long polymer. This is evident in the solid curves of Figures 12 and 13, showing the behavior of pure long polymer: the storagelike response ($-\omega^2\Psi'_{1,L}$) is almost completely flat and the dissipative response ($\omega^2\Psi''_{1,L}$) falls with increasing frequency. With the addition of short chains to the blends, a mode of relaxation of the long chains with a peak frequency equal to that of pure short polymer loss peak is predicted in the model. This relaxation is manifested in $-\omega^2\Psi'_{1,L}$ as a decrease from the high-frequency plateau with decreasing ω and in $\omega^2\Psi''_{1,L}$ by the appearance of a peak occurring at the same frequency as the peak in the corresponding pure short-polymer spectrum (Figure 15). The magnitude of the long-chain relaxation in this high-frequency domain increases linearly with the volume fraction of short polymer in the blend.

When local orientational coupling is present, the dichroism spectra of long-chain labeled blends are predicted by eq 5.15 to be a superposition of the long-chain orientation at the level of statistical segments (Figures 12 and 13) and the mean-field orientation (Figure 2b and 3b). For the case $\epsilon = 0.3$, the resulting predictions for the long-chain dichroism spectra (Figures 5b and 6b) are similar to the long-chain contribution to the stress (Figures 12 and 13). Because the high-frequency relaxation of the bulk is greater than that of the long chains in the blend, the superposition of the two gives a slightly greater reduction in $-\omega^2L'$ than in $-\omega^2\Psi'_{1,L}$ with decreasing frequency and higher and broader peaks in ω^2L'' than in $\omega^2\Psi''_{1,L}$ of the blends.

The short-chain contribution to the real and imaginary parts of the amplitude of the first normal stress difference $-\omega^2\Psi'_{1,S}$ and $\omega^2\Psi''_{1,S}$ are shown in Figures 14 and 15. All of the $-\omega^2\Psi'_{1,S}$ spectra fall from a common high-frequency plateau through zero and to negative values as the frequency decreases to below 1 rad/s. Pure short polymer relaxes most sharply, changing sign at a frequency of 3 rad/s, higher than the short chains in the blends. With the addition of long polymer to the blend, short-chain relaxation slows, moving the frequency at which $-\omega^2\Psi'_{1,S}$ becomes negative to lower values and the terminal region (where the magnitude of $-\omega^2\Psi'_{1,S}$ falls as ω^2 with decreasing frequency) shifts to the left. The qualitative shape of $-\omega^2\Psi'_{1,S}$ is, nevertheless, the same for the blends and pure short polymers. Similar trends are seen in the effect of blend composition on $\omega^2\Psi''_{1,S}$. The pure short polymer shows a single, broad peak with a maximum at 10 rad/s; with addition of long polymer to the blend, this peak shifts to the left and drops more sharply on the low-frequency side.

There is a stark contrast between the short-chain contributions to Ψ^*_1 and the short-chain dichroism predicted in the case of orientational coupling with $\epsilon = 0.3$, especially between $-\omega^2\Psi'_{1,S}$ in Figure 14 and $-\omega^2S'$ in Figure 7b. The most striking difference is that not all of the $-\omega^2S'$ dichroism spectra change sign; those that do show a strong dependence of the frequency at which $-\omega^2S'$ changes sign on Φ_L. In addition, at low frequency $-\omega^2S'$ becomes positive again for $\Phi_L = 0.1$, 0.2, and 0.3. The reason that the effect of orientational coupling is so glaring is that it produces local orientation (leading to dichroism $-\omega^2S'$, Figure 7b) of the short chains in a frequency regime ($\omega < 1$ rad/s) that is so slow that the corresponding larger scale orientation of the short chains (responsible for $-\omega^2\Psi'_{1,S}$, Figure 14) has almost completely relaxed. The contrast between ω^2S'' (Figure 8b) and $\omega^2\Psi''_{1,S}$ (Figure 15) is not so pronounced. The main difference being that instead of the low-frequency relaxation with a power of the frequency that is independent of Φ_L observed for $\omega^2\Psi''_{1,S}$, the response of the dichroism ω^2S'' at $\omega < 0.5$

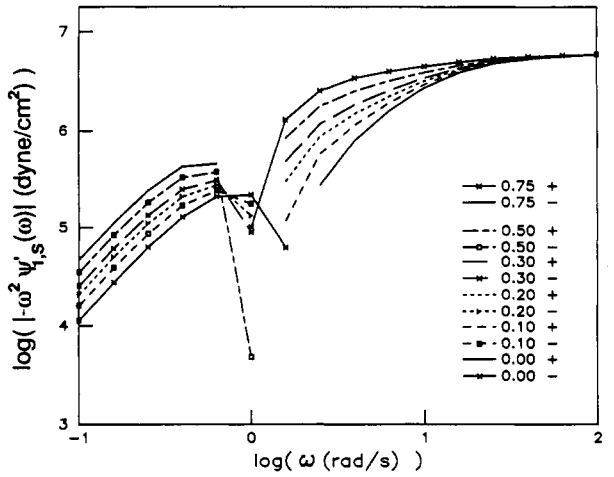

Figure 14. Predicted contribution of the short chains to the real part of the complex amplitude of the first normal stress difference.

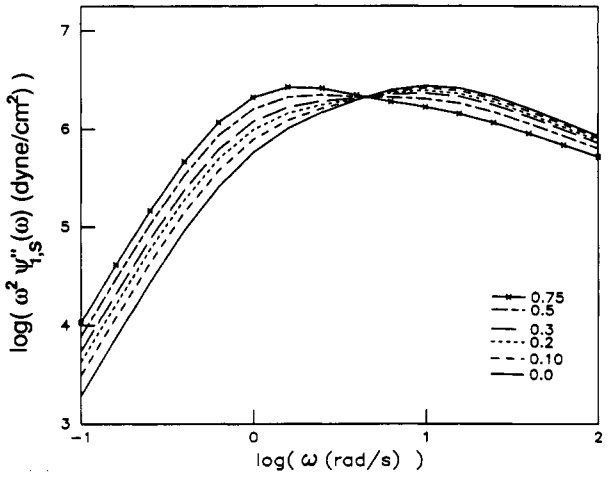

Figure 15. Predicted contribution of the short chains to the imaginary part of the complex amplitude of the first normal stress difference.

rad/s decays with decreasing frequency more slowly as Φ_L increases. In fact, for $\Phi_L = 0.75$, $\omega^2 S''$ passes through a minimum and begins to increase with decreasing frequency at the lower limit of the range of interest ($\omega = 0.1$ rad/s).

Finally, the agreement between the observed dichorism spectra (Figures 7a and 8a) and the predicted dichroism spectra (Figure 7b and 8b) is good; much better than the agreement between the observed dichroism and the predicted component contributions to the normal stress (Figures 14 and 15). This is especially evident from the comparison of the observed $-\omega^2 S'$ spectra and the model prediction for $-\omega^2 S'$ in parts a and b of Figure 7 with Figure 14, the model prediction for $-\omega^2 \Psi'_{1,S}$.

References and Notes

(1) Ninomiya, K.; Ferry, J. D. *J. Colloid Sci.* **1963**, *18*, 421.
(2) Masuda, T.; Kitagawa, K.; Inoue, T.; Onogi, S. *Macromolecules* **1970**, *2*, 116.
(3) Kurata, M.; Osaki, K.; Einaga, Y.; Sugie, T. *J. Polym. Sci., Polym. Phys. Ed.* **1974**, *12*, 849.
(4) Struglinski, M. J.; Graessley, W. W. *Macromolecules* **1985**, *18*, 2630.
(5) Doi, M.; Edwards, S. F. *J. Chem. Soc., Faraday Trans. 2* **1978**, *74*, 1789, 1802, 1818.
(6) Graessley, W. W. *Adv. Polym. Sci.* **1982**, *47*, 67.
(7) Daoud, M.; de Gennes, P.-G. *J. Polym. Sci., Polym. Phys. Ed.* **1979**, *17*, 1971.
(8) Marrucci, M. *J. Polym. Sci., Polym. Phys. Ed.* **1985**, *23*, 159.
(9) Viovy, J. L. *J. Phys. (Les Ulis., Fr.)* **1985**, *46*, 847.
(10) Rubinstein, M.; Colby, R. H. *J. Chem. Phys.* **1988**, *89*, 5291.
(11) Watanabe, H.; Tirrell, M. *Macromolecules* **1989**, *22*, 927.
(12) Rubinstein, M.; Helfand, E.; Pearson, D. S. *Macromolecules* **1987**, *20*, 822.
(13) des Cloizeaux, J. *Macromolecules* **1990**, *23*, 4678.
(14) Kornfield, J. A.; Fuller, G. G.; Pearson, D. S. *Macromolecules* **1989**, *22*, 1334.
(15) Kornfield, J. A.; Fuller, G. G.; Pearson, D. S. *Rheol. Acta* **1990**, *29*, 105.
(16) Bird, R. B.; Armstrong, R. C.; Hassager, O. *Dynamics of Polymeric Liquids*; John Wiley & Sons: New York, 1987; Vol. 1.
(17) Janeschitz-Kriegl, H. *Polymer Melt Rheology and Flow Birefringence*; Springer-Verlag: New York, 1983.
(18) Spriggs, T. W.; Huppler, J. D.; Bird, R. B. *Trans. Soc. Rheol.* **1966**, *10*, 191.
(19) Thulstrup, E. W.; Michl, J. *J. Am. Chem. Soc.* **1982**, *104*, 5594.
(20) Matsuoka, Y. *J. Phys. Chem.* **1980**, *84*, 1361.
(21) Schmidt, P.; Schneider, B. *Makromol. Chem.* **1983**, *184*, 2075.
(22) Jacobi, M. M.; Stadtler, R.; Gronski, W. *Macromolecules* **1986**, *19*, 2884.
(23) Sotta, P.; Deloche, B.; Herz, J.; Lapp, A.; Durand, D.; Rabadeux, J.-C. *Macromolecules* **1987**, *20*, 2769.
(24) Queslel, J.-P.; Erman, B.; Monnerie, L. *Polymer* **1988**, *29*, 1818.
(25) Jarry, J.-P.; Monnerie, L. *Macromolecules* **1979**, *12*, 316.
(26) Doi, M.; Pearson, D. S.; Kornfield, J. A.; Fuller, G. G. *Macromolecules* **1989**, *22*, 1488.
(27) Merrill, W. W.; Tirrell, M.; Jarry, J.-P.; Monnerie, L. *Macromolecules* **1989**, *22*, 896.
(28) Pearson, D. S. *Rubber Chem. Technol.* **1987**, *60*, 439.
(29) Prest, W. M.; Porter, R. S. *Polym. J.* **1973**, *4*, 154.
(30) de Gennes, P.-G. *J. Chem. Phys.* **1971**, *55*, 572.
(31) de Gennes, P.-G. *Scaling Concepts in Polymer Physics*; Cornell University Press: Ithaca, NY, 1979.
(32) Doi, M.; Graessley, W. W.; Helfand, E.; Pearson, D. S. *Macromolecules* **1987**, *20*, 1900.
(33) Green, P. F.; Kramer, E. J. *Macromolecules* **1986**, *19*, 1108.
(34) Verdier, P. H.; Stockmayer, W. H. *J. Chem. Phys.* **1962**, *36*, 227.
(35) Orwoll, R. A.; Stockmayer, W. H. *Adv. Chem. Phys.* **1969**, *15*, 305.
(36) Rouse, P. E. *J. Chem. Phys.* **1953**, *21*, 1272.
(37) Ylitalo, C. M.; Kornfield, J. A.; Fuller, G. G.; Pearson, D. S. *Macromolecules* **1991**, *24*, 749.
(38) DiMarzio, E. A. *J. Chem. Phys.* **1962**, *36*, 1563.
(39) Jackson, J. L.; Shen, M. C.; McQuarrie, D. A. *J. Chem. Phys.* **1966**, *44*, 2388.
(40) Kornfield, J. A. Measurement and Theory of the Dynamics of Polydisperse Polymer Melts. Ph.D. Dissertation, Stanford University, Stanford, CA, Dec 1988.